Aerospace Science and Technology 76 (2018) 72–81

Contents lists available at ScienceDirect

Aerospace Science and Technology

www.elsevier.com/locate/aescte

Influence of repetitive laser pulse energy depositions on supersonic flow over a sphere, cone and oblate spheroid

Ahmad Rezaei Sangtabi [a], Abas Ramiar [b,*], Ali Akbar Ranjbar [b], M. Abdollahzadeh [c,d], Ali Kianifar [a]

[a] Ferdowsi University of Mashhad, Mashhad, Iran
[b] Babol University of Technology, Babol, P.O. Box 484, Iran
[c] Departamento de Engenharia Electromecanica, C-MAST – Center for Mechanical and Aerospace Sciences and Technologies, Universidade da Beira Interior, Covilha, Portugal
[d] Department of Mechanical Engineering, Amirkabir University of Technology (Tehran Polytechnic), Tehran, 15875-4413, Iran

ARTICLE INFO

Article history:
Received 11 May 2017
Received in revised form 7 December 2017
Accepted 1 February 2018
Available online 6 February 2018

Keywords:
Laser deposition
Drag reduction
Flow control
Supersonic flow

ABSTRACT

In this work, numerical simulation of active flow control of high speed flows by means of unsteady laser energy deposition was conducted. Supersonic flow over a sphere, cone and oblate spheroid was studied. The effect of single and multiple laser pulses on reduction of the drag force over these aerodynamic nose shapes were studied and compared. In addition, the effect of Mach number, location of energy deposition, number of laser pulses and the frequency of energy deposition were studied. A solver was developed for OpenFOAM to simulate the compressible flow at high Mach numbers. The shock capturing property of the solver was improved using AUSM+-up to calculate the pressure and velocity fluxes at the cell faces. For the validation purpose, simulation of the unsteady laser energy deposition in supersonic flow over a sphere was compared with experimental data. The results of single laser pulse deposition indicated that the interaction of the blast wave and bow shock leads to increase in the drag force. However, when the total laser energy was divided to smaller energy pulses and was applied at high frequency, the maximum drag force was decreased significantly and duration of drag reduction was increased. In addition, it was observed that by increasing the number of laser pulses and the distance between the energy deposition location and body, the duration of drag reduction was increased. In the end, energy saving efficiency for all the simulated cases was calculated. The energy saving efficiency was increased significantly by an increase in the free stream Mach number in spite of the decrease in the duration of drag reduction phase. For the conditions tested here, the maximum energy saving efficiency for supersonic flow over a cone was 65%, while it reached to as high as 750% and 460% for supersonic flow over a sphere and oblate spheroid.

1. Introduction

The study of supersonic flow control over blunt bodies is important in the field of aerospace engineering. The nose shape of many high speed projectiles, rockets and missiles approximately features a blunt body which suffers from excessive heating loads and drag forces [1,2]. Along with design optimization studies for the leading edge shapes [3–5], flow control is necessary to decrease the pressure and heat fluxes at the stagnation points and to reduce the wave drag of a hypersonic vehicle. As one of the typical flow control methods, a physical spike is connected to the body nose. Although this method significantly reduces the drag, in a flight condition with an angle of attack, this will generate pitching moment as well as large heat flux at the apex of the spike. To overcome these problems, active flow control methods have been investigated. In these methods, energy deposition by means of electric, microwave and laser discharge are applied ahead of the supersonic vehicle to generate a blast wave. The interaction of the blast wave and the bow shock modifies the shock structure and reduces the pressure on the front surface of the body. Adelgren et al. [6–8] experimentally studied the effects of energy deposition induced by a single laser pulse in a supersonic flow over a sphere at $M = 3.45$. Their results demonstrated that single laser pulse can reduce 40% of the peak pressure value, compared to the value measured without energy deposition. Zheltovodov et al. [9, 10] used 2D axisymmetric unsteady Euler equations to investigate the interaction of a single laser pulse with a sphere in the air-

* Corresponding author.
E-mail address: aramiar@nit.ac.ir (A. Ramiar).

https://doi.org/10.1016/j.ast.2018.02.005
1270-9638/

Nomenclature

a	Speed of sound	$m\,s^{-1}$
d	Distance between laser discharge and body	m
D	Base Diameter	m
e	Internal energy	J
E	Total energy per unit volume	$J\,m^{-3}$
$\boldsymbol{E}$	Vector of conservative variables	
f	Frequency	Hz
f_a	Scaling factor	
$\boldsymbol{F}$	Vector of numerical fluxes	
$\boldsymbol{G}$	Vector of numerical fluxes	
$\boldsymbol{H}$	Vector of numerical fluxes	
H_t	Total enthalpy	J
L	Length of low density region	m
$\dot{m}$	Mass flux	kg/s
M	Mach number	
n	Number of pulses	
p	Pressure	Pa
Q	Total deposited energy	J
q	Energy of pulses	J
R	Gas constant	J/kg K
t	Time	s
T	Temperature	K
U	Velocity	m/s
u	Velocity in x direction	$m\,s^{-1}$
v	Velocity in y direction	$m\,s^{-1}$
V_∞	Free stream velocity	$m\,s^{-1}$

Greek symbols

η	Energy saving efficiency	
θ	vertex angle, degree	
ρ	Density	$kg\,m^{-3}$

Subscript

0	Reference
1/2	Cell interface
L	Left state
R	Right state
ss	Steady state
w	blast wave
∞	Free stream

Abbreviations

PIMPLE	Merged PISO-SIMPLE
PISO	Pressure implicit with splitting of operator
SIMPLE	Semi-Implicit Method for Pressure Linked Equations
AUSM	Advection Upstream Splitting Method

flow at $M = 3.45$. The laser energy deposition was modeled by considering a specific distribution for energy deposition density. They have studied the effects of a single and periodic pulse energy deposition in the argon flow and compared their results with available experimental data. Azarova and Knight [11–13] numerically studied the effect of microwave discharge and laser energy deposition on the supersonic flow past a hemisphere–cylinder and hemisphere–cone–cylinder at Mach 2.1 and 3.45. In order to model the energy deposition, they used a channel of low density gas at the inflow boundary condition. They observed that the effect of microwave discharge is the generation of a longitudinal homogeneous region of heated gas ahead of the body. Lashkov et al. [14] conducted an experimental and numerical study on the efficiency of microwave energy deposition in a supersonic flow past a blunt body at various Mach numbers. For the simulation of energy deposition, the energy corresponding to that absorbed by microwave discharge was deposited in a cylindrical region. They observed that a short microwave impulse can result in significant streamlining of blunt body and considerable drop in the drag. Also, they showed that the efficiency of microwave energy deposition is enhanced with increasing Mach number. Azarova [15] modeled the Richtmyer–Meshkov and Kelvin–Helmholtz instabilities as a result of an energy release on the supersonic flow past a cylindrical body. They have used a heated rarefied channel for simulating the effect of energy deposition. They reported that the density stratified vortex and the Richtmyer–Meshkov instability in front separation area lead to reduction of the drag force. Abdollahzadeh et al. [16–18] numerically studied the influence of nanosecond dielectric barrier discharge on the flow structure. The nanosecond pulse voltage used to transfer energy from plasma to a fluid which leads to the formation of micro-shock waves and therefore to the modification of flow features. The energy deposition by nanosecond dielectric barrier discharge was modeled by considering a heated region near the surface of the actuator. Ogino et al. [19,20] investigated the effects of single pulse energy deposition on drag reduction in a supersonic flow field around a sphere. Their results showed that the energy saving efficiency had a linear dependence on the radius of the low density core formed in the blast wave and was proportional to the square of the free stream Mach number. Yanji et al. [21] used laser energy to break down the hypersonic flow in a shock tunnel and solved 3D Navier–Stokes equations to compare experimental and numerical simulation results at $M = 5$. They showed that by high rate laser energy deposition, the pressure and temperature at the stagnation point and the wave drag are reduced to 50%, 75% and 81% respectively. Sasoh et al. [22] used high frequency repetitive laser pulse energy deposition to study the drag characteristics of truncated cones in $M = 1.94$ flow. Their results showed that with employing a concave head and increasing the laser pulse repetition frequency, the drag decrement is enhanced. Sasoh et al. [23] measured the drag over a flat-nosed cylinder with a repetitive laser pulse in a $M = 2$, in-darf wind tunnel. The efficiency of energy deposition that was defined as the ratio between a decrement in the necessary propulsion power to the incident power, reached over 1000%. Mortazavi and Knight [24] simulated the interaction of laser-discharged plasma with a hemisphere at Mach 3.45. They solved unsteady compressible Navier–Stokes equations with the commercial software GASPex. The numerical results from the viscous and inviscid perfect gas models compared with the experimental data and indicated that the boundary layer thickness is very small compared to the diameter of the hemisphere and the viscous effects are very negligible in the energy deposition simulation at high Mach numbers. Joarder et al. [25] used Helmholtz free-energy minimization to investigate the effect of laser energy deposition ahead of a semicircular body. Their simulation results showed reserve flow, bow shock lensing, vortex and a low pressure region ahead of the body. They determined the pressure, temperature and species composition of the laser energy deposition zone after cessation of the laser pulse. They found that the average wave drag decreases with the increase in laser energy.

According to the literature, several parameters are influencing the flow control capacity of the laser energy deposition. Some of the reviewed articles have discussed the effect of some of these parameters. However, there is not yet a comprehensive comparison of the effects of these parameters. In this paper, the influence of free stream Mach number, laser pulse repetition frequency, number of the laser pulses and the energy deposition location on the

energy deposition efficiency is investigated. In addition, in order to compare and study the effect of laser energy deposition on the flow control around different geometries, interaction of the blast wave with the bow and oblique shocks, energy deposition into supersonic flow over a sphere, cone and oblate spheroid is simulated. In the end, energy saving efficiency for different conditions is calculated and presented.

2. Governing equations and numerical model

The 2D axisymmetric Euler equations were employed to simulate the supersonic flow over the considered blunt bodies, which can be written as:

$$\frac{\partial \boldsymbol{E}}{\partial t}+\frac{\partial \boldsymbol{F}}{\partial x}+\frac{\partial \boldsymbol{G}}{\partial y}=0 \tag{1}$$

with

$$\boldsymbol{E}=\begin{pmatrix}\rho\\ \rho u\\ \rho v\\ \rho E\end{pmatrix},\qquad \boldsymbol{F}=\begin{pmatrix}\rho u\\ \rho u^2+p\\ \rho uv\\ (\rho E+p)u\end{pmatrix},$$

$$\boldsymbol{G}=\begin{pmatrix}\rho v\\ \rho uv\\ \rho v^2+p\\ (\rho E+p)v\end{pmatrix} \tag{2}$$

where, u and v denote the x and y velocity components. ρ, p and E are the gas density, pressure and total energy per unit volume. E is determined as:

$$E=e+\frac{1}{2}\left(u^2+v^2\right) \tag{3}$$

where, e is the internal energy of gas per unit volume. The density is related to the pressure and temperature by the equation of state:

$$p=\rho RT \tag{4}$$

where, R and T are the gas constant and temperature, respectively. The working fluid was air and was assumed to be a perfect gas with constant specific heat ratio of 1.4.

The governing equations were solved with the *sonicFoam* solver of OpenFOAM [26]. The above equations were discretized using the finite volume method [27]. Due to importance of shock capturing in supersonic flow condition, a high resolution scheme, namely the GAMMA differencing scheme [28] was employed for the discretization of the spatial terms. Also, the first order implicit Euler scheme was used for the discretization of the temporal term. The PIMPLE algorithm, which is a combination of SIMPLE and PISO algorithms, was used to couple the continuity and momentum equations. The PIMPLE algorithm [29] benefits from the speed and precision of the PISO algorithm and the convergence of the SIMPLE. In the PIMPLE algorithm, larger Courant numbers than PISO can be used in transient solutions. It consists of two main inner and outer loops. In the outer loop (predictor step or PIMPLE loop), the density and velocity fields are calculated by solving an explicit and an implicit version of the continuity and momentum equations. The relaxation factor is used in the pimple loop except the last one and again set to the value assigned at the start of the simulation to ensure the time consistency. That is, the pressure–momentum coupling is calculated k times, in which it is calculated $(k-1)$ times with relaxation (like SIMPLE) and the last time without relaxation [29]. In the inner loop (correction step or PISO loop), the pressure and total energy equations are solved implicitly. When a thermodynamic property varies rapidly in a short time (for example laser discharge), the energy equation is located in the inner loop in order to improve the pressure-temperature coupling [30]. In the end of inner loop, the velocity and density fields are updated by explicit expressions.

To improve the shock capturing property of the solver, the AUSM$^+$-up [31,32] flux definition was used to obtain the fluxes at the control volume faces. The formulation of AUSM+-up can be found in [33] with full details and here, it is described briefly. The interface velocity ($U_{1/2}$) is determined by:

$$U_{1/2}=M_{1/2}a_{1/2} \tag{5}$$

At the interface, left state and right state speed of sound can be obtained as follows:

$$a_{1/2}=\min(\hat{a}_{\mathrm{L}},\hat{a}_{\mathrm{R}}) \tag{6}$$

$$\hat{a}_{\mathrm{L}}=\frac{(a^*)^2}{\max(a^*,U_{\mathrm{L}})},\qquad \hat{a}_{\mathrm{R}}=\frac{(a^*)^2}{\max(a^*,-U_{\mathrm{R}})} \tag{7}$$

a^* is the critical speed of sound and for a perfect gas can be expressed as:

$$a^*=\sqrt{\frac{2(\gamma-1)}{\gamma+1}H_t} \tag{8}$$

The left and right Mach numbers are given by:

$$M_{\mathrm{L/R}}=\frac{U_{\mathrm{L/R}}}{a_{1/2}} \tag{9}$$

Liou [33] introduced a scaling factor (f_a) as a function of the reference Mach number (M_0) to properly scale the numerical dissipation. This factor is applied to scale the pressure and velocity diffusion terms.

$$f_a(M_0)=M_0(2-M_0)\geq 0\quad f_a\approx 2M_0\quad \text{if } M_0\to 0 \tag{10}$$

$$M_0^2=\min\left(1,\max\left(\overline{M}^2,M_\infty^2\right)\right) \tag{11}$$

$$\overline{M}^2=\left(M_{\mathrm{L}}^2+M_{\mathrm{R}}^2\right)/2 \tag{12}$$

With these values, the interface Mach number ($M_{1/2}$) is determined as:

$$M_{1/2}=M_{(4)}^{+}(M_{\mathrm{L}})+M_{(4)}^{-}(M_{\mathrm{R}})+M_p \tag{13}$$

$$M_{(4)}^{\pm}(M)=\begin{cases}M_{(2)}^{\pm}(M)(1\mp 16\beta M_{(2)}^{\mp}(M)) & |M|<1\\ M_{(1)}^{\pm}(M) & |M|\geq 1\end{cases} \tag{14}$$

$$M_{(1)}^{\pm}(M)=\frac{1}{2}\left(M\pm|M|\right) \tag{15}$$

$$M_{(2)}^{\pm}(M)=\pm\frac{1}{4}(M\pm 1) \tag{16}$$

$$M_p=-\frac{K_p}{f_a}\max\left(1-\overline{M}^2,0\right)\frac{p_{\mathrm{R}}-p_{\mathrm{L}}}{\rho_{1/2}a_{1/2}^2} \tag{17}$$

where $\rho_{1/2}=(\rho_{\mathrm{R}}+\rho_{\mathrm{L}})/2$. The pressure flux ($p_{1/2}$) is given as follows:

$$p_{1/2}=p_{(5)}^{+}(M_{\mathrm{L}})p_{\mathrm{L}}+p_{(5)}^{-}(M_{\mathrm{R}})p_{\mathrm{R}}+p_u \tag{18}$$

$$p_{(5)}^{\pm}(M)=\begin{cases}M_{(2)}^{\pm}(M)[(\pm 2-M)\mp 16\varphi M M_{(2)}^{\mp}(M)] & |M|<1\\ \frac{1}{M}M_{(1)}^{\pm}(M) & |M|\geq 1\end{cases} \tag{19}$$

$$p_u=-k_u p_{(5)}^{+}(M_{\mathrm{L}})p_{(5)}^{-}(M_{\mathrm{R}})(\rho_{\mathrm{R}}+\rho_{\mathrm{L}})a_{1/2}f_a(U_{\mathrm{R}}-U_{\mathrm{L}}) \tag{20}$$

$$\varphi=\frac{3}{16}\left(-4+5f_a^2\right)\in\left[-\frac{3}{4},\frac{3}{16}\right] \tag{21}$$

The mass flux is obtained from the following relation:

$$\dot{m}_{1/2} = \frac{1}{2}\left[U_{1/2}(\rho_R + \rho_L) - |U_{1/2}|(\rho_R - \rho_L)\right] \quad (22)$$

In the present study, we set $k_p = 0.25$, $k_u = 0.75$, $\beta = 1/8$.

According to the literature review presented in the introduction section, there are two widely used methods for simulating the effect of laser energy deposition. In one approach, energy deposition is modeled via creation of a heated rarefied channel ("filament [13]"). This low density channel is applied instantaneously in the flow field for simulation of energy deposition effects. The length and diameter of the channel, gas density in the channel are set in such a way that the results resemble the experiments. However, there are few drawbacks in adopting this approach. The first peak of the drag force after interacting of the blast wave (resulted from the laser energy deposition) and the bow shock (on the blunt body) is not observed in the simulation of the interaction between a low density channel and the bow shock [12]. In addition, overlapping of these low channels may occur in the repetitive laser pulse energy deposition. In the second approach, the simulation of energy deposition is considered only as a heated region. It is assumed that a portion of the deposited energy increases the temperature/internal energy of the heated region [34]. This last approach does not have the mentioned drawbacks of considering a low density channel and therefore it is adopted here for simulating the effect of laser energy deposition.

The simulation of energy deposition by the laser discharge is performed in two stages. First, the steady state solution of supersonic flow over the body is obtained. Then, the laser discharge is added to the steady state solution as an instantaneous creation of a heated region with increased temperature and pressure. Assumption of the instantaneous deposition of the laser energy is reasonable, since the width of the laser pulse (10 ns) [6,21] is very small compared to the time scale of flow. The laser energy is deposited uniformly in the spherical region with radius $r_0 = 0.9$ mm. The temperature distribution in the heated region is determined by:

$$\begin{cases} T = T_{ss} + \Delta T & r < r_0 \\ T = T_{ss} & r > r_0 \end{cases} \quad (23)$$

where r is the spherical radius measured from the center of the heated region. Similar to [34], multiple simulations with different values of ΔT were performed in order to determine the value of ΔT that the computed results are in best agreement with the experimental normalized pressure. Then, the equation of state is used to obtain the pressure in the discharge region. Since the laser discharge is instantaneous, the velocity and density remain constant in the heated region.

3. Boundary conditions

The two dimensional planer graph of the geometries and computational domain are shown in Fig. 1. In this figure, D represents the base diameter of the considered geometries and it is kept constant $D = 25.4$ mm. d represents the distance between the body and the center of the energy deposition location, which was varied between $0.8D$ to $1.2D$. The deposited energy changes from 283 to 28.3 mJ. For all the cases, static pressure and temperature of the free stream flow were set to 13.1 kPa and 77.8 K respectively, which were defined according to the experiment of Adelgren et al. [6]. All variables were prescribed at the inlet and were extrapolated at the outlet. The slip boundary condition was applied to the surface of the body. The axis of symmetry was applied on the x-axis. The wedge boundary condition was applied to the back and front boundaries.

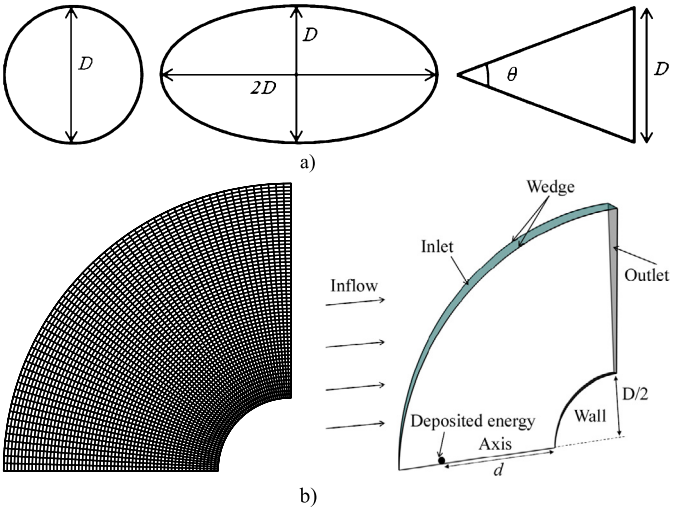

Fig. 1. Schematic of a) Geometry of test cases and b) Computational domain and boundary conditions for the simulation of energy deposition in supersonic flow.

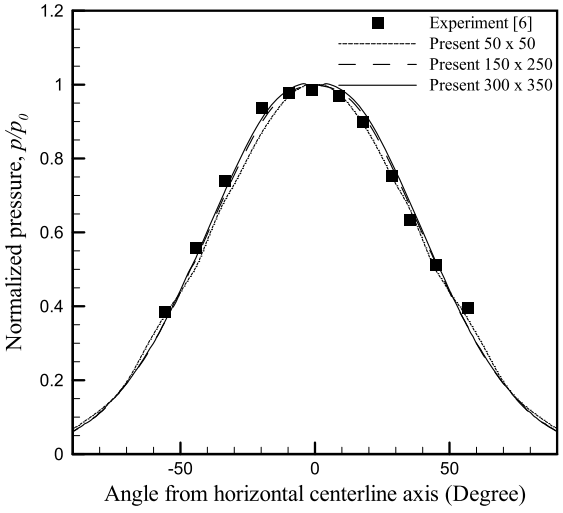

Fig. 2. Grid independence study based on the ratio of pressure on the sphere (p) to the stagnation pressure (p_0).

4. Validation

The validation case was adapted from the experiments of Adelgren et al. [6]. The computational domain for this case is similar to the one shown in Fig. 1b. The diameter of sphere D is 25.4 mm. The distance between the body and the center of the energy deposition location is equal to the sphere diameter. The deposited energy is 283 mJ. Since the simulation of energy deposition by the laser discharge involves a preliminary steady state simulation before energy deposition and a post transient simulation after deposition of the localized laser energy, the adapted numerical methodology and solver must be validated separately for both steady state and transient simulations. For steady state simulation, the supersonic flow past a sphere at Mach 3.45 was considered. To analyze the grid independence of the solution, three meshes with different grid densities were employed. Fig. 2 compares the normalized pressure (p/p_0) obtained from the numerical simulation, which is the ratio of pressure on the sphere (p) to the stagnation pressure on the centerline of the blunt body (p_0), with the experimental data [6]. The normalized pressure on the sphere surface using a grid density of greater than 150×250 becomes independent of the grid scale. Another parameter that can be compared with the experimental data is the standoff distance, which is the distance

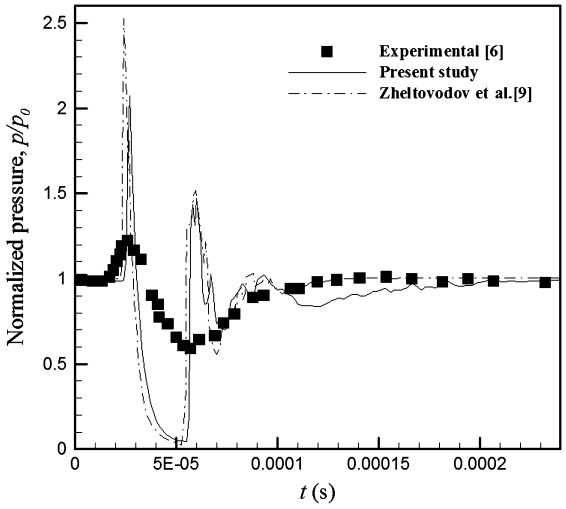

Fig. 3. The time history of normalized pressure at the center of sphere with $Q = 283$ mJ, $n = 1$, $d = D$, $M = 3.45$.

between the front face of the shock wave and the stagnation point. Our numerical result predicted the standoff distance within 2 percent of the measured distance [35].

The above steady state solution was used as the initial condition for the energy deposition simulation. Then, a laser energy of $Q = 283$ mJ was deposited/released on upstream of the blunt body. In Fig. 3, the time history of the pressure variation at the center of sphere that is normalized by the stagnation pressure without laser discharge is compared with the experimental data [6] and the numerical simulation of Zheltovodov et al. [9]. The disagreement between the numerical and experimental results was also reported in the previous numerical studies. Ignoring the molecular ionization [21] and chemical transformations [11], the interaction of the laser generated plasma with the body [34] and the insufficient precision experimental data [9,11] were reported as the reasons for the disagreement between the simulation and experimental results.

Fig. 4 shows the time sequences of instantaneous schlieren images [6] and the simulated density contours for laser energy deposition. As seen in Fig. 4, the calculated structures of the flow field matches well with the experiment. The blast wave is formed after laser energy deposition in upstream of the body (Fig. 4a). When the blast wave impinged on the bow shock and reflected at the blunt body, a transmission shock is generated. The transmission shock compresses the flow and a local high pressure region is formed (Fig. 4b). The low density core of the blast wave interacts with the bow shock and the bow shock is deformed while the gas in the shock layer is pulled upstream. Deformation of the bow shock is called the lens effect [36] (Fig. 4c). As a result, the bow shock wave is distorted near the stagnation point and low pressure region is formed behind it. At this time, body drag and the pressure at the stagnation point is significantly decreased. The interaction of the upstream section of the blast wave with the bow shock causes an increase in the pressure at the front of the body (Fig. 4d).

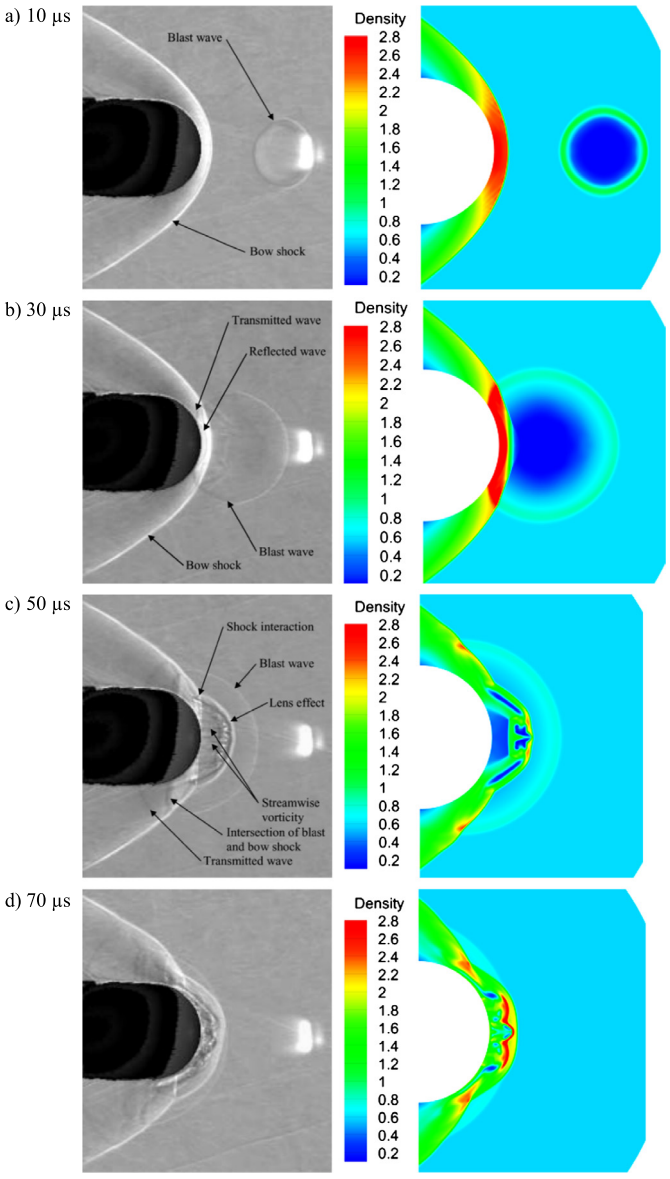

Fig. 4. Comparison of time sequences of the schlieren images reported in [6] (left) and gas density contours obtained from the numerical simulation for laser energy deposition (right). (For interpretation of the colors in this figure, the reader is referred to the web version of this article.)

5. Results and discussion

5.1. Effect of energy deposition mode ($Ma = 3.45$, $d = D$)

Simulations of single laser pulse deposition were performed for the cone with vertex angle of $\theta = 60°$ and the oblate spheroid with the aspect ratio of 2:1 (ratio of major to minor axes) at the constant base diameter $D = 25.4$ mm. The time history of the normalized drag (D_t/D_{ss}), which is the ratio of instantaneous drag force to the one without energy deposition is presented in Fig. 5.

Fig. 5 shows a small increase in the drag force after the interaction of blast wave with oblique shock. The maximum normalized drag reduction for laser deposition over a cone was smaller than the sphere and oblate spheroid. Fig. 6 shows the pressure contours obtained from simulations of single laser energy deposition in the supersonic flow over the oblate spheroid and cone. In Fig. 6a, a high pressure region was formed in the front of the blunt body after the interaction of blast wave and shock wave. This high pressure region in the front of oblate spheroid leads to an increase in the drag force. Due to the absence of this high-pressure region on the tip of the cone, drag force was increased insignificantly. The formation of low pressure region caused by lens effect in front of the oblate spheroid is shown in Fig. 6b. This phenomenon, which led to a sharp reduction in the drag force, is not seen in the interaction of the blast wave and oblique shock. The high pressure region formed by the interaction of the upstream of the blast wave and bow shock is displayed in Fig. 6c. This region is not formed in

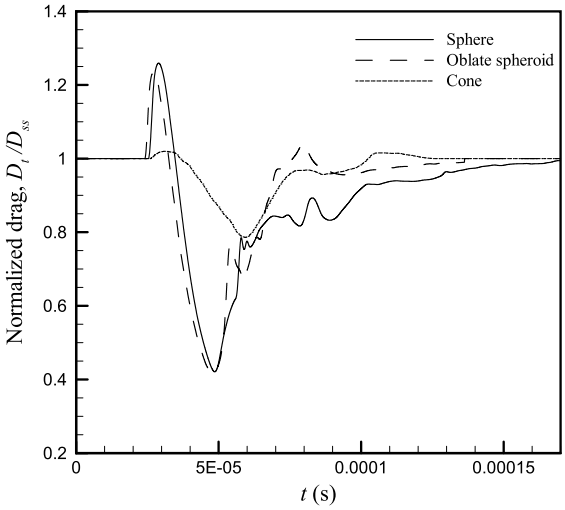

Fig. 5. Normalized drag force as a function of time for deposition of a single laser pulse with $Q = 283$ mJ, $n = 1$, $d = D$, $M = 3.45$.

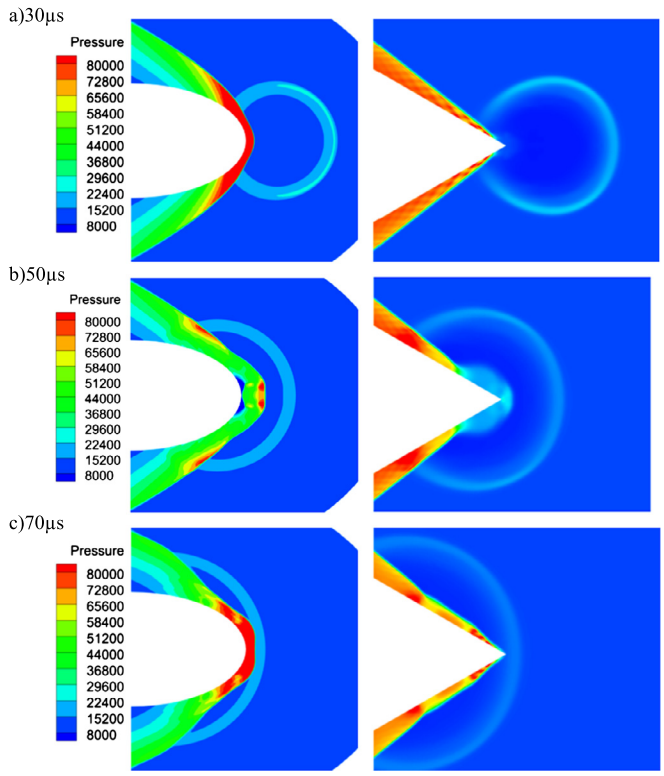

Fig. 6. Pressure contours obtained from numerical simulation of energy deposition in the supersonic flow over the spheroid and cone with $Q = 283$ mJ, $n = 1$, $d = D$, $M = 3.45$. (For interpretation of the colors in this figure, the reader is referred to the web version of this article.)

the flow over the cone and therefore the drag force is increased smoothly unlike the flow over blunt bodies.

Although using a single laser energy pulse significantly decreases the drag force, but the duration of the low pressure region is quite short. Therefore, the first peak of the drag force is high and the drag force after lens effect increases quickly on the blunt body. To overcome these problems, the high rate repetition of the same deposited energy was used as suggested in [21]. The total laser energy was divided to five equal pulses $q = 56.6$ mJ and applied by frequencies of $f = 50$ kHz and $f = 100$ kHz. The time history of the normalized drag for the case of repetitive laser energy deposition is given in Fig. 7. Using high rate pulses for laser energy deposition, duration of wave drag reduction was increased while the peak of the initial increment in the wave drag was decreased. At the frequency $f = 50$ kHz, as seen in Fig. 7, after each interaction the bow shock had enough time to reform and interact with the next wave. Therefore, the peak of the wave drag was decreased and the duration of drag reduction was increased compared to a single pulse. But after the lens effect of each pulse, the drag force was sharply increased on the body. With increasing the frequency of laser pulse repetition to $f = 100$ kHz, the duration of drag decrement is reduced, and the drag force fluctuation between the maximum and minimum values becomes weaker.

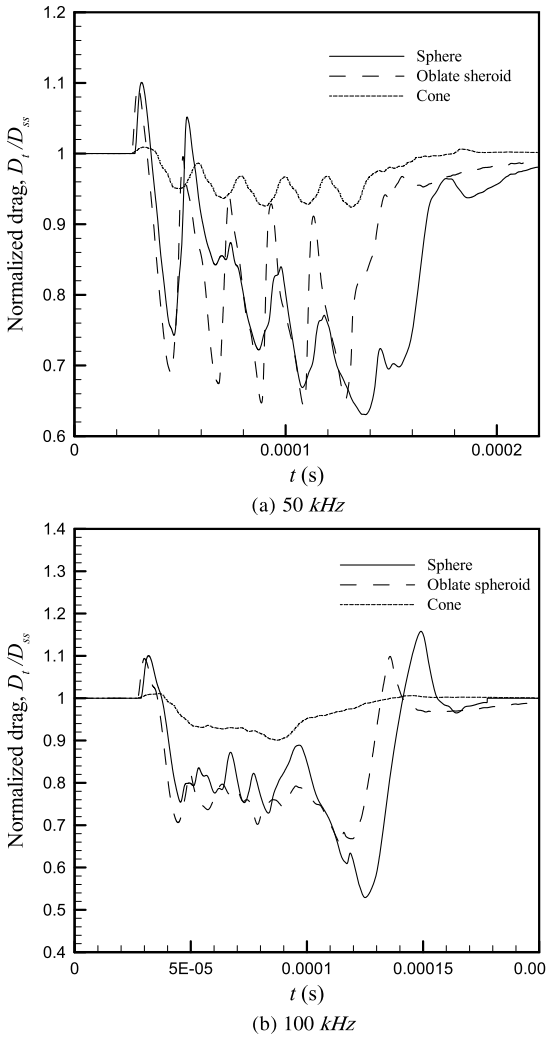

Fig. 7. Time history of normalized drag for high rate repetitive laser energy deposition with $q = 56.6$ mJ, $d = D$, $n = 5$, $M = 3.45$.

The density contours for different frequencies are shown in Fig. 8. A space between the two low density region was observed at frequency of $f = 50$ kHz ($t = 30$ μs). After interaction between the first low density core with bow shock, a high density/pressure region forms at the front of the blunt body ($t = 45$ μs) and interacts with the second low density region which leads to a high pressure region on the blunt body surface ($t = 55$ μs).

Fig. 9 plots the normalized drag as a function of time for the case when the total laser energy is divided to the ten equal pulses of $q = 28.6$ mJ and is applied by frequencies of $f = 50$ kHz and $f = 100$ kHz. Comparison between Fig. 7b and Fig. 9 shows that there was no significant difference between maximum drag force decrement in the two simulations, but the duration of the drag

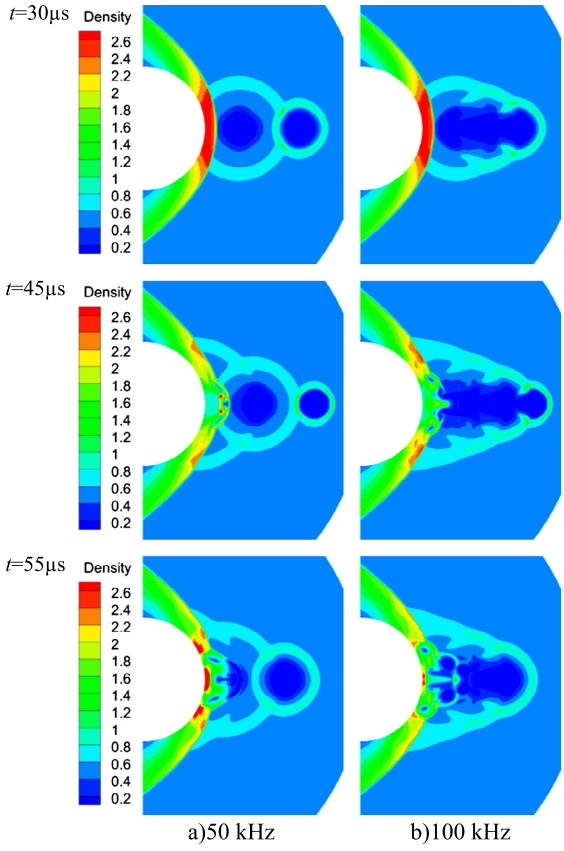

Fig. 8. Density contours obtained from numerical simulation of repetitive laser energy deposition in the supersonic flow over the sphere with $Q = 56.6$ mJ, $n = 5$, $d = D$, $M = 3.45$. (For interpretation of the colors in this figure, the reader is referred to the web version of this article.)

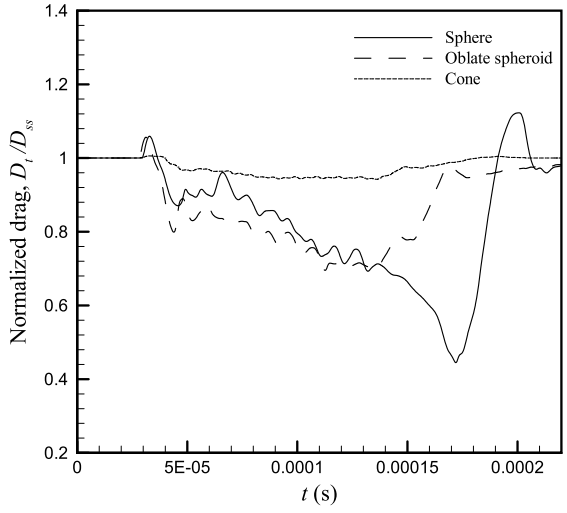

Fig. 9. Time history of the normalized drag for $q = 28.3$ mJ, $f = 100$ kHz, $n = 10$, $d = D$, $M = 3.45$.

reduction in the case of $q = 28.6$ mJ (ten pulses) was longer than $q = 56.6$ mJ (five pulses).

5.2. Effect of the location of laser energy deposition

The distance between energy deposition location and the body (d) is another important parameter influencing the flow control using laser energy deposition. The effect of the energy deposition location on the normalized drag is plotted in Fig. 10 for

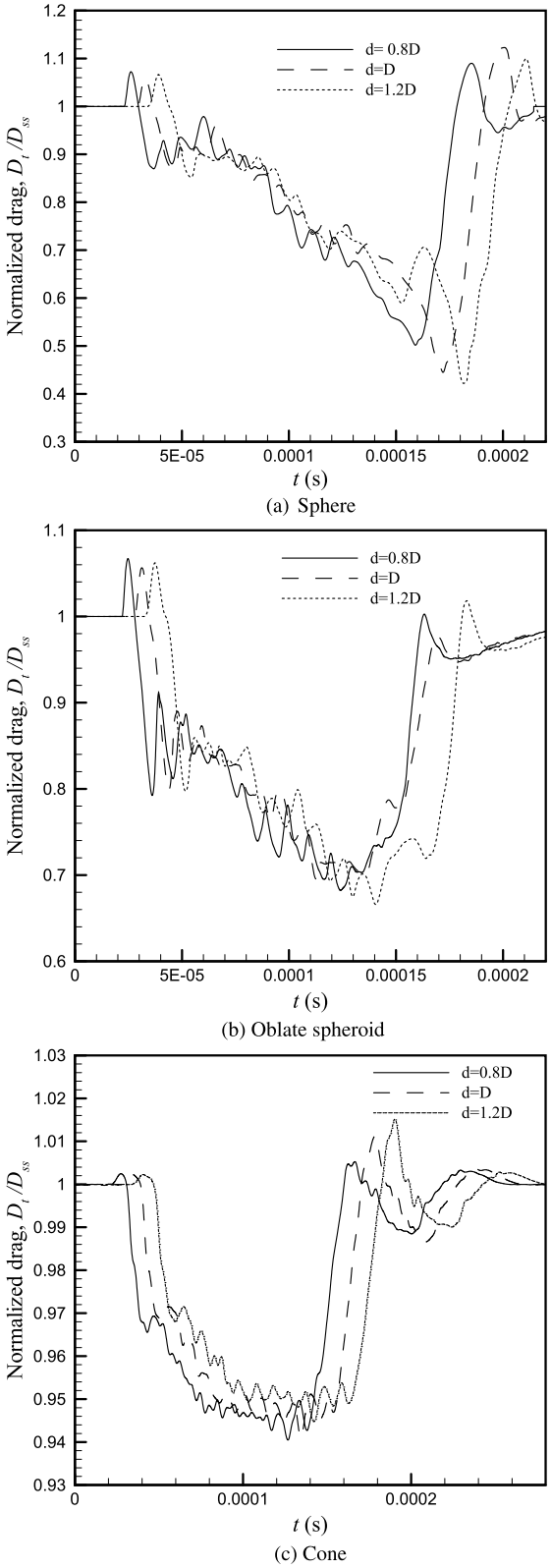

Fig. 10. Time history of the normalized drag for a) sphere b) oblate spheroid c) cone. $q = 28.3$ mJ, $f = 100$ kHz, $n = 10$, $M = 3.45$.

$f = 100$ kHz, $M = 3.45$, $n = 10$. The diameter of the low density region increases and surrounds the body as the laser energy deposition is placed farther from the body. Fig. 11 shows the effect of the energy deposition location on the blast wave diameter after the interaction with the bow shock. As seen in Fig. 11a, the diam-

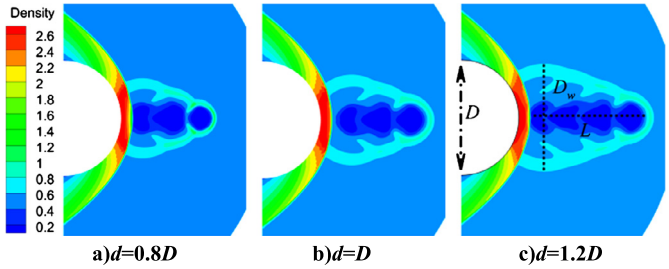

Fig. 11. Effect of energy deposition location on the blast wave diameter for $q = 28.6$ mJ, $n = 10$, $d = D$, $M = 3.45$. (For interpretation of the colors in this figure, the reader is referred to the web version of this article.)

eter of the blast wave (D_w) is smaller than the diameter of sphere (D). Fig. 11c shows that the diameter of blast wave and the length of the low density region (L) increase as the distance between the energy deposition location and the sphere increases. Consequently, the body moves into the low density region for more time and the maximum drag reduction increases (Fig. 10a).

5.3. Effect of free stream Mach number

Fig. 12 compares the effect of free stream Mach number in terms of time history of normalized drag for sphere, Oblate spheroid and cone for laser energy deposition with $d = D$, $n = 10$, $f = 100$ kHz. When the free stream Mach number increases, the blast wave moves faster and interacts with the bow shock in a shorter time. At higher Mach numbers, the diameter of the low density core decreases and the bow shock has a longer time to reform after each interaction with the blast waves. In addition at high Mach numbers, as seen in Fig. 12, the duration of the drag reduction is shorter and the decrease in the normalized drag is smaller than lower Mach numbers. But, this does not mean that the energy deposition is optimal at low Mach numbers due to the fact the drag forces are normalized by their steady state values (without laser energy deposition). The steady state drag on the sphere, oblate spheroid and cone was increased by 189% (from 30.816 N to 89.28 N), 159% (from 21.6 N to 55.944 N) and 143% (from 20.376 N to 57.6 N) as the free stream Mach number was changed from 2.5 to 5. Therefore, it can be concluded that the drag reduction with laser energy deposition is more effective at high Mach number. In the next section, the efficiency of laser energy deposition for the above simulations was calculated.

5.4. Energy saving efficiency of laser energy deposition

The energy saving efficiency, which is given by the ratio of the energy saving due to drag reduction to the sum of the repetitively supplied energy, is calculated as:

$$\%\eta = \frac{\int V_\infty D_0 (1 - D/D_0)\, dt}{Q} \times 100 \tag{24}$$

Drag force increment after the interaction of bow shock with blast wave (the negative value of the term $(1 - D/D_0)$), the duration of drag reduction (dt), the steady drag force (D_0) and the free stream Mach number (V_∞) are four effective factors in the energy saving efficiency. The energy saving efficiency for the cases presented in the previous section is given in Table 1. Results shows that by using several laser pulses instead of a single pulse, the flow control performance can be improved. Although, the increase in frequency of the pulse repetition decreases the time that the drag is reduced, the energy saving efficiency demonstrates a different behavior with the increase in frequency. The efficiency is decreased when the blast wave interacts with the bow shock. The interaction of the blast wave with the oblique shock caused an increase in the energy saving efficiency. When five and ten pulses were applied by frequency of $f = 50$ kHz instead of a single pulse at the constant total energy, the energy saving efficiency for the laser discharge on upstream of the sphere was increased by 82% and 128%, respectively. The results showed that increasing the number of pulses

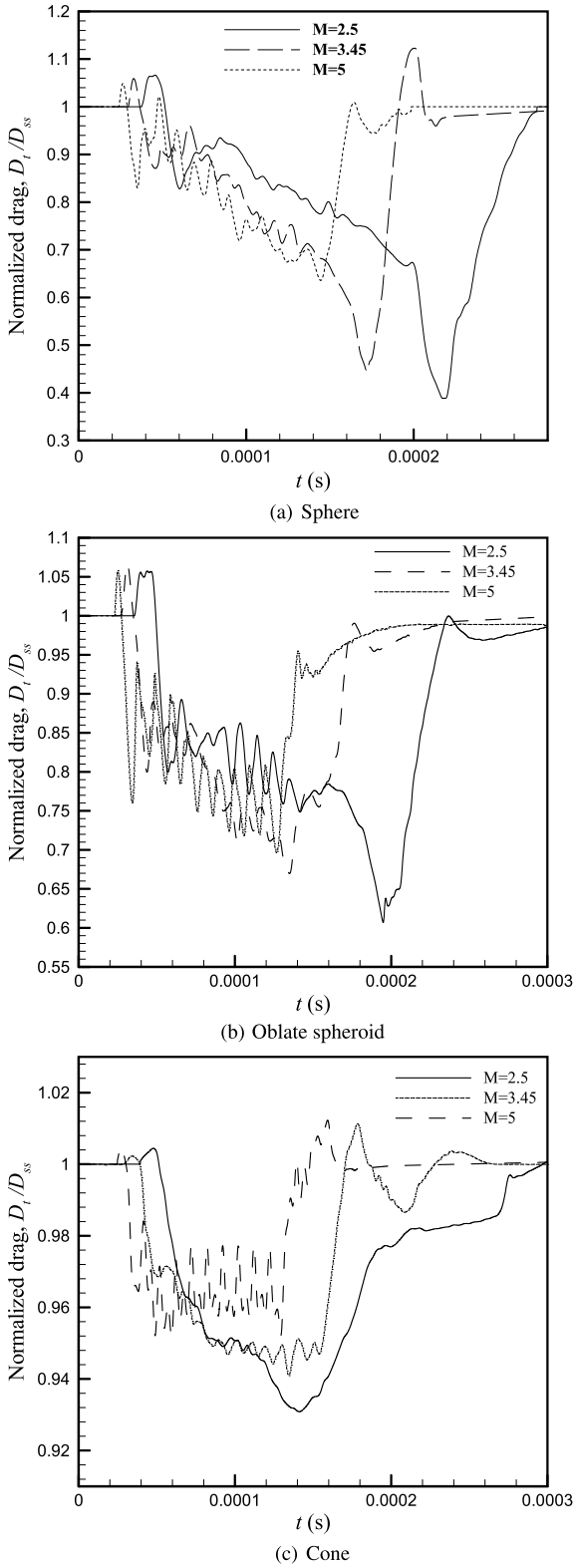

Fig. 12. Time history of the normalized drag at different free stream Mach number for $q = 28.6$ mJ, $f = 100$ kHz, $n = 10$, $d = D$.

Table 1
Energy saving efficiency with constant total energy ($Q = 283$ mJ).

Operation conditions	Variable parameter	Energy saving efficiency		
		Sphere	Oblate spheroid	Cone
$M = 3.45$	Single pulse	199	93	24.4
$d = D$ (25.4 mm)	$n = 5$ pulses	363	184	35.9
$f = 50$ kHz	$n = 10$ pulses	454	226	40
$M = 3.45$	Single pulse	199	93	24.4
$d = D$ (25.4 mm)	$n = 5$ pulses	267	179	40.7
$f = 100$ kHz	$n = 10$ pulses	415	221	46.4
$M = 3.45$	$d = 0.8D$	396	214	47.1
$n = 10$	$d = D$	415	221	46.4
$f = 100$ kHz	$d = 1.2D$	451	240	45.3
$d = D$	$M = 2.5$	240	132	31
$n = 10$	$M = 3.45$	415	218	46.4
$f = 100$ kHz	$M = 5$	750	416	65

from one to ten at a frequency of 50 kHz causes an increase in the energy saving efficiency by 143% and 64% for oblate spheroid and cone, respectively. As seen in Table 1, 8.6%, 2.2% decrease and 16% increase in the energy saving efficiency were observed when the frequency changes from 50 kHz to 100 kHz for the sphere, oblate spheroid and cone, respectively. The proportion between efficiency and frequency for flow over a cone is in accordance with the results of Saosh et al. [22]. The efficiency of energy deposition is increased as the energy is released in a farther location from bow shock and closer to the oblique shock. When the distance between body and energy deposition point was increased from $0.8D$ to $1.2D$, the efficiency was increased by 14% and 12% for sphere and oblate spheroid and was decreased by 3.8% for the cone. Due to higher steady drag force, an increase in the free stream Mach number improved the energy saving efficiency in spite of the decrease in the duration of the time that the drag is reduced. The simulation results showed that the efficiency of the laser discharge was increased by 212%, 215% and 110% for the sphere, oblate spheroid and cone as the free stream Mach number changes from 2.5 to 5. Based on the Eq. (24), for a constant free stream Mach number and the laser deposited energy, reduction of the drag force is the only factor which is influencing the energy saving efficiency. According to Fig. 5, the reduction of the normalized drag force for the cone shape is lower (and thus the energy saving efficiency) compared to the other two cases (sphere and oblate spheroid cases). The reason for this difference on the level of drag reduction is explained in Fig. 6. The lens effect (caused from the interaction of the bow shock and the blast wave) forms a low pressure region in front of the blunt shape object. This will lead to sharp reduction of the drag force. However, this phenomenon is not observed in the interaction of the blast wave and the oblique shock and thus a low pressure region is not seen in front of the cone. Therefore the reduction of the drag force for the cone case is lower compared to the sphere and oblate spheroid cases.

6. Conclusions

In this study, a compressible solver for the solution of high Mach number flow was implemented. The PIMPLE algorithm was used in order to couple the velocity–pressure–temperature fields. In order to improve the shock capturing characteristic of the solver, the AUSM+-up flux definition was employed to obtain the velocity and pressure fluxes at the cell faces. The algorithm was tested initially for the steady state supersonic flow over a sphere. The accuracy of the solution was verified by comparing the results of the present study with the experimental data found in the literature. Subsequently, the steady state solution was used as an initial condition for the simulation of unsteady laser energy discharge into supersonic flow over the sphere. The time history of normalized pressure obtained from the numerical simulation was compared with experimental results. Next, the effects of frequency, the number of pulses, location of energy deposition and free stream Mach number on the drag force in the supersonic flow over a sphere, oblate spheroid and cone were studied. In the end, the energy saving efficiency for different conditions was calculated. From the obtained results, following observations may be summarized:

Number of pulses: The energy saving efficiency for a single pulse of $Q = 283$ mJ was 199%, 93% and 24% for supersonic flow past a sphere, oblate spheroid and cone, respectively. By splitting total energy into multiple pulses with lower energy, the drag reduction duration increases. When total energy was divided into 10 smaller pulses ($f = 50$ kHz), the energy saving efficiency was increased by 128%, 143% and 64% for sphere, oblate spheroid and cone, respectively.

Frequency: At lower frequency, high pressure regions formed after each interaction of blast wave and bow shock. The drag reduction duration was increased and the drag force fluctuations were damped as the frequency was changed from 50 kHz to 100 kHz. Energy saving efficiency was decreased by 8.6% and 2.2% for sphere and oblate spheroid. A 16% increase in the energy saving efficiency was observed as the frequency was changed from 50 kHz to 100 kHz. In addition, an average 15% increase in the energy saving efficiency was observed when the frequency changed from 50 kHz to 100 kHz for deposited energy of 28.3 mJ. The results observed here are in accordance with the results reported in [21,22].

Free stream Mach number: Unlike the steady state drag force, the drag reduction duration is inversely proportional to the free stream Mach number. The steady state drag force on the sphere, oblate spheroid and cone increased from 30.816 N, 21.6 N and 20.376 to 89.28 N, 55.944 N and 57.6 N as the free stream Mach number changed from 2.5 to 5. When free stream Mach number was changed form 2 to 5, the energy saving efficiency was improved by 212%, 215% and 110% for supersonic flow over a sphere, oblate spheroid and cone, respectively.

Energy deposition location: The diameter of blast wave/low density region increases as the distance between energy deposition location with the body increases. An average of 14% and 12.15% increase in the efficiency for interaction of blast waves with bow shock was observed as the deposition point was changed from $0.8D$ to $1.2D$ for the case of cases of sphere and Oblate spheroid respectively. At this condition, the efficiency decreased by 4% for supersonic flow over a cone.

Shape of the body: Utilization of laser energy deposition of the all the shapes including the blunt shapes (sphere and Oblate spheroid) and the cone case resulted in effective reduction of the drag force. For the cone case, the reduction of the drag force was lower compared to the blunt shapes. The reason is ascribed to the difference in the interaction of the blast wave (formed due to laser energy deposition) and the bow shock (for blunt shape bodies) and the oblique shock (for the cone case) and to the absence of formation of low pressure region ahead of the cone shape body.

Conflict of interest statement

None declared.

References

[1] W. Huang, Z. Zhao, L. Yan, Y. Zhou, R. Zhang, Parametric study on the drag and heat flux reduction mechanism of forward-facing cavity on a blunt body in supersonic flows, Aerosp. Sci. Technol. 71 (2017) 619–626.

[2] W. Huang, L. Yan, J. Liu, L. Jin, J.G. Tan, Drag and heat reduction mechanism in the combinational opposing jet and acoustic cavity concept for hypersonic vehicles, Aerosp. Sci. Technol. 42 (2015) 407–414.
[3] W.S. Hinman, S. Schmitt, C.T. Johansen, P.E. Rodi, L.M. Corporation, Computational fluid dynamics study of optimized hypersonic leading edge geometries, in: 20th AIAA Int. Sp. Planes Hypersonic Syst. Technol. Conf, 2015, pp. 1–13.
[4] K. Kontogiannis, A. Cerminara, N. Taylor, A. Soberster, N. Sandham, Parametric geometry models for hypersonic aircraft components: blunt leading edges, in: 20th AIAA Int. Sp. Planes Hypersonic Syst. Technol. Conf, 2015, pp. 1–20.
[5] P. Rodi, Optimization of Bezier curves for high speed leading edge geometries, in: 51st AIAA Aerosp. Sci. Meet. Incl. New Horizons Forum Aerosp. Expo, 2013, pp. 1–17.
[6] R.G. Adelgren, H. Yan, G.S. Elliott, D.D. Knight, T.J. Beutner, A.A. Zheltovodov, Control of Edney IV interaction by energy pulse, AIAA J. 43 (2005) 256–269.
[7] R.G. Adelgren, G.S. Elliott, D.D. Knight, A.A. Zheltovodov, T.J. Beutner, Energy deposition in supersonic cavity flow, in: 42nd AIAA Aerosp. Sci. Meet. Exhib, 2001, pp. 1–33.
[8] R. Adelgren, H. Yan, G. Elliott, D. Knight, A. Zheltovodov, M. Ivanov, Localized flow control by laser energy deposition applied to Edney IV and intersecting shocks, in: 41st Aerosp. Sci. Meet. Exhib, 2003, pp. 1–37.
[9] A.A. Zheltovodov, E.A. Pimonov, D.D. Knight, Energy deposition influence on supersonic flow over axysimmetric bodies, in: 45th AIAA Aerosp. Sci. Meet. Exhib., 2007, pp. 1–31.
[10] A.A. Zheltovodov, E.A. Pimonov, D.D. Knight, Supersonic vortex breakdown control by energy deposition, in: AIAA 43rd Aerosp. Sci. Meet, 2005, pp. 1–36.
[11] O.A. Azarova, D.D. Knight, Numerical prediction of dynamics of interaction of laser discharge plasma with a hemisphere–cylinder in a supersonic flow, in: 53rd AIAA Aerosp. Sci. Meet, 2015, pp. 1–12.
[12] O.A. Azarova, D.D. Knight, Interaction of microwave and laser discharge resulting "heat spots" with supersonic combined cylinder bodies, Aerosp. Sci. Technol. 43 (2015) 343–349.
[13] O.A. Azarova, D.D. Knight, An approach of drag force decrease for combined cylinder AD bodies under the action of microwave and laser energy deposition, Aerosp. Sci. Technol. 64 (2017) 154–160.
[14] V.A. Lashkov, A.G. Karpenko, R.S. Khoronzhuk, I.C. Mashek, Effect of Mach number on the efficiency of microwave energy deposition in supersonic flow, Phys. Plasmas 23 (2016) 1–6.
[15] O.A. Azarova, Generation of Richtmyer–Meshkov and secondary instabilities during the interaction of an energy release with a cylinder shock layer, Aerosp. Sci. Technol. 42 (2015) 376–383.
[16] M. Abdollahzadeh, J.C. Páscoa, P.J. Oliveira, Numerical investigation on efficiency increase in high altitude propulsion systems using plasma actuators, in: Proc. Eur. Congr. Comput. Methods Appl. Sci. Eng, 2012, pp. 6563–6581.
[17] M. Abdollahzadeh, F. Rodrigues, J.C. Pascoa, P.J. Oliveira, Numerical design and analysis of a multi-DBD actuator configuration for the experimental testing of ACHEON nozzle model, Aerosp. Sci. Technol. 41 (2015) 259–273.
[18] M. Abdollahzadeh, J.C. Pascoa, P.J. Oliveira, Two-dimensional numerical modeling of interaction of micro-shock wave generated by nanosecond plasma actuators and transonic flow, J. Comput. Appl. Math. 270 (2014) 401–416.
[19] Y. Ogino, N. Ohnishi, S. Taguchi, K. Sawada, Baroclinic vortex influence on wave drag reduction induced by pulse energy deposition, Phys. Fluids 21 (2009) 1–11.
[20] Y. Ogino, M. Tate, N. Ohnishi, Shock control with baroclinic vortex induced by a pulse energy deposition, in: 47th AIAA Aerosp. Sci. Meet. Incl. New Horizons Forum Aerosp. Expo, 2009, pp. 1–11.
[21] H. Yanji, W. Diankai, L. Qian, Y. Jifei, Interaction of single-pulse laser energy with bow shock in hypersonic flow, Chin. J. Aeronaut. 27 (2014) 241–247.
[22] A. Sasoh, J.H. Kim, K. Yamashita, T. Sakai, Supersonic aerodynamic performance of truncated cones with repetitive laser pulse energy depositions, Shock Waves 24 (2014) 59–67.
[23] A. Sasoh, Y. Sekiya, T. Sakai, J. Kim, A. Matsuda, Supersonic drag reduction with repetitive laser pulses through a blunt body, AIAA J. (2010) 2811–2817.
[24] M. Mortazavi, D. Knight, Numerical simulation of energy deposition in a viscous supersonic flow past a hemisphere, in: 53rd Aerosp. Sci. Meet, 2015, pp. 1–10.
[25] R. Joarder, U.P. Padhi, A.P. Singh, H. Tummalapalli, Two-dimensional numerical simulations on laser energy depositions in a supersonic flow over a semi-circular body, Int. J. Heat Mass Transf. 105 (2017) 723–740.
[26] H.G. Weller, G. Tabor, A tensorial approach to computational continuum mechanics using object-oriented techniques, Comput. Phys. 12 (1998) 620–631.
[27] J.H. Ferziger, M. Peric, Computational Methods for Fluid Dynamics, 2002.
[28] H. Jasak, H.G. Weller, A.D. Gosman, High resolution NVD differencing scheme for arbitrarily unstructured meshes, Int. J. Numer. Methods Fluids 31 (1999) 431–449.
[29] V.H. Bhusare, M.K. Dhiman, D.V. Kalaga, S. Roy, J.B. Joshi, CFD simulations of a bubble column with and without internals by using OpenFOAM, Chem. Eng. J. 317 (2017) 157–174.
[30] M. Abdollahzadeh, J.C. Pascoa, P.J. Oliveira, Implementation of the classical plasma–fluid model for simulation of dielectric barrier discharge (DBD) actuators in OpenFOAM, Comput. Fluids 128 (2016) 77–90.
[31] C.M. Xisto, J.C. Páscoa, P.J. Oliveira, A pressure-based method with AUSM-type fluxes for MHD flows at arbitrary Mach numbers, Int. J. Numer. Methods Fluids 72 (2013) 1165–1182.
[32] C.M. Xisto, J.C. Páscoa, P.J. Oliveira, D.A. Nicolini, A hybrid pressure-density-based algorithm for the Euler equations at all Mach number regimes, Int. J. Numer. Methods Fluids 70 (2012) 961–976.
[33] M.S. Liou, A sequel to AUSM, Part II: AUSM$^+$-up for all speeds, J. Comput. Phys. 214 (2006) 137–170.
[34] M. Mortazavi, D. Knight, Numerical simulation of energy deposition in a supersonic flow past a hemisphere, in: 52nd Aerosp. Sci. Meet, 2014, pp. 1–10.
[35] M.D. Van Dyke, The supersonic blunt-body problem – review and extension, AIAA J. 25 (1958) 485–496.
[36] P.Y. Georgievskii, V.A. Levin, Unsteady interaction of a sphere with atmospheric temperature inhomogeneity at supersonic speed, Fluid Dyn. 28 (1993) 568–574.